

UC Irvine

UC Irvine Previously Published Works

Title

The Virus Bioresistor: Wiring Virus Particles for the Direct, Label-Free Detection of Target Proteins

Permalink

<https://escholarship.org/uc/item/2pv8248k>

Journal

Nano Letters, 18(6)

ISSN

1530-6984

Authors

Bhasin, Apurva
Ogata, Alana F
Briggs, Jeffrey S
et al.

Publication Date

2018-06-13

DOI

10.1021/acs.nanolett.8b00723

Peer reviewed



Published in final edited form as:

Nano Lett. 2018 June 13; 18(6): 3623–3629. doi:10.1021/acs.nanolett.8b00723.

The Virus BioResistor: Wiring Virus Particles for the Direct, Label-Free Detection of Target Proteins

Apurva Bhasin^{1,†}, Alana F. Ogata^{1,†}, Jeffrey S. Briggs², Phillip Y. Tam², Ming X. Tan³, Gregory A. Weiss^{1,2,*}, and Reginald M. Penner^{1,2,*}

¹Department of Chemistry, University of California, Irvine, Irvine, CA 92697-2025

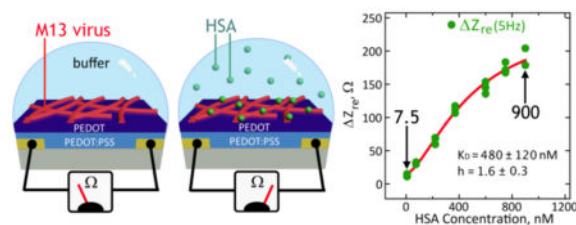
²PhageTech Inc., 5 Mason, Suite 170, Irvine, CA 926187

³Wainamics Inc., 3135 Osgood Ct, Fremont, CA 94539

Abstract

The virus bioresistor (*VBR*) is a chemiresistor that directly transfers information from virus particles to an electrical circuit. Specifically, the *VBR* enables the label-free detection of a target protein that is recognized and bound by filamentous M13 virus particles, each with dimensions of 6 nm (*w*) × 1 μm (*l*), entrained in an ultra-thin (≈250 nm) composite virus-polymer resistor. Signal produced by the specific binding of virus to target molecules, is monitored using the electrical impedance of the *VBR*: The *VBR* presents a complex impedance that is modeled by an equivalent circuit containing just three circuit elements: a solution resistance (R_{soln}), a channel resistance (R_{VBR}), and an interfacial capacitance (C_{VBR}). The value of R_{VBR} , measured across five orders of magnitude in frequency, is increased by the specific recognition and binding of a target protein to the virus particles in the resistor, producing a signal R_{VBR} . The *VBR* concept is demonstrated using a model system in which human serum albumin (HSA, 66 kDa) is detected in a phosphate buffer solution. The *VBR* cleanly discriminates between a change in the electrical resistance of the buffer, measured by R_{soln} and selective binding of HSA to virus particles, measured by R_{VBR} . The R_{VBR} induced by HSA binding is as high as 200 Ω, contributing to low sensor-to-sensor coefficients-of-variation (<15%) across the entire calibration curve for HSA from 7.5 nM to 900 nM. The response time for the *VBR* is 3 – 30 seconds.

Graphical abstract



[†]These authors contributed equally to this work.

Supporting Information

The Supporting Information is available free of charge on the ACS Publications website at DOI: 10.1021/acs.nano-lett.8b00289. Detailed description of experimental methods including VBR fabrication, impedance measurements, AFM and SEM analysis, and virus receptor selection.

Keywords

Bacteriophage; chemiresistor; biosensor; impedance; human serum albumin

Investigating the electrical properties of microscopic biological entities such as organelles, bacteria, eukaryotic cells, and viruses is both interesting from a fundamental science perspective, as well as challenging because they are electrically insulating. How does one “wire” such structures to an external circuit?^{1,2,3} Elegant solutions to this problem have been demonstrated involving interfaces to single cells, bacteria etc. involving single nanostructures or ensembles of nanostructures (nanowires, nanotubes, nanosheets, etc.). For example, electrical signals from single cells have been measured using graphene field-effect transistors, and nanowire-embedded n-p junctions.^{4,5} The “wiring” of bacteria to electrode surfaces has been accomplished using outer sphere redox mediators.^{6,7,8}

A new approach, the *virus bioresistor* (or *VBR*), provides the means for incorporating virus particles into an electrical circuit (Figure 1). The key to the *VBR* is an electronically conductive channel composed of poly(3,4-ethylenedioxythiophene) or PEDOT into which M13 virus particles are embedded (Figure 1a). Individual M13 virus particles are filamentous with dimensions of 6 nm (w) × 1.0 μm (l). The recognition and binding of target molecules to thousands of M13 virus particles embedded in this polymeric channel is signaled by an electrical impedance signature, which can be measured by an external circuit (Figure 1b,c). The impedance response of the *VBR* is modeled by a simple equivalent circuit containing just three circuit elements: A solution resistance (R_{soln}), a channel resistance (R_{VBR}), and an interfacial capacitance (C_{VBR}) (Table 1). Information on target binding is contained in the R_{VBR} , which can be measured either at a single frequency or from the best fit of the Nyquist plot across 40 or 50 discrete frequencies using this equivalent circuit.

We demonstrate the *VBR* concept using a model system in which human serum albumin (HSA, 66 kDa), is detected in a phosphate buffer solution. The *VBRs* described here have a baseline dc resistance of 200–250 Ω which is the same in air or in an aqueous buffer solution, and are capable of producing large signals ($R_{VBR} \approx 250 \Omega$, or $R_{VBR}/R_o \approx 100\%$) for the detection of HSA in phosphate buffer solutions across the entire HSA binding curve ranging from [HSA] = 7.5 to 900 nM. In spite of the fact that the electrical signal generated by *VBRs* derives purely from ensembles of biological entities, extremely high sensor-to-sensor reproducibility of this signal is attainable for the response of *VBR* biosensors culminating in a coefficient-of-variation of the measured [HSA] for 20 sensors less than 15% across the entire HSA binding curve. The *VBR* achieves these metrics using a two-terminal, monolithic device architecture that is simple, robust, manufacturable, and inexpensive. No reagents and no sandwich amplification of the impedance signal are required, and no redox species are added to the test solution. Collectively, these data demonstrate the feasibility of adapting the *VBR* concept to rapid, inexpensive urine and blood-based assays at the point-of-care.

The fabrication of a *VBR* involves the preparation of two gold electrical contacts on a glass substrate by photolithography (Figure 2). On top of these contacts, a two-layer *VBR* channel (15 mm (l) × 20 mm (w)) is prepared consisting of a spin-cast PEDOT-PSS semiconductor

bottom layer (200–300 nm in thickness) and an electrodeposited virus-PEDOT composite top layer containing thousands of engineered M13 virus particles^{9,10,11} (90 – 100 nm in thickness). This virus-PEDOT electrodeposition process involves the application of two oxidizing voltammetric scans to an aqueous solution containing 8 nM M13 virus particles in 12.5 mM LiClO₄, 2.5 mM EDOT (Figure 3a).

If the PEDOT-PSS/PEDOT-virus layer that electrically connects the two metal electrodes is severed, forcing current traveling between these two electrodes into the solution phase, we recently demonstrated that the resulting device still functions as a biosensor.²⁰ But the *VBR* has three attributes not found in this device: 1). An impedance signal that is amplified by a factor of 20 (200 Ω here *versus* 12 Ω in our prior work.²⁰ The result is a limit-of-detection of 7.5 nM in the *VBR* versus 100 nM in the earlier device,²⁰ 2) The ability to decouple this signal from the salt concentration of the solution (*vide infra*), and, 3) A dramatically faster response time of ≈5 s here *versus* 8–10 min.²⁰

A cross-sectional SEM image of a *VBR* biosensor film shows a virus-PEDOT top layer with a thickness of ~92 nm on top of a ~245 nm PEDOT:PSS bottom layer (Figure 3b). Plain-view SEMs of pure PEDOT films prepared in an aqueous plating solution of 2.5 mM EDOT and 12.5 mM LiClO₄ show a smooth, homogenous surface (Figure 3c). Virus-PEDOT films prepared from the same plating solution with the addition of 8 nM virus show dark, filamentous structures within the virus-PEDOT top layer (Figure 3d). These filaments are M13 bacteriophage, which have typical dimensions of 6 nm (diameter) × 1.0 μm (length). Atomic force microscopy (AFM) images show that in the absence of virus particles, the virus-PEDOT top layer is smooth with an RMS surface roughness of 5 nm (Figure 3e,g). If this layer is produced to contain virus particles, a slightly rougher surface is seen with an RMS roughness of 10 nm; however, a distinct topography reveals the presence of fiber like structures that can be attributed to PEDOT-covered virus strands protruding from the PEDOT surface (Figure 3f,h). After the virus-PEDOT top layer is electrodeposited, the bioaffinity layer is complete, and the *VBR* is ready to use.

We elected to monitor *VBR*s using an *ac* impedance measurement, rather than applying a simpler *dc* resistance measurement, because prior work on conductive polymer based chemiresistors have shown conclusively that dramatically lower noise can be accessed using *ac* detection, even at frequencies as low as 5 Hz.^{12,13,14} Analytical equations for the real and imaginary components of the complex impedance, Z_{re} and Z_{im} (Table 1), are used to fit experimental impedance data to extract the values of the three circuit elements: R_{soln} , R_{VBR} , and C_{VBR} . A version of the equivalent circuit in which a constant phase element (CPE) is substituted for each capacitor is used for this purpose. This elaboration provides better agreement between the calculated and the experimental impedance data, resulting in improved precision for the measurement of R_{VBR} (Table 1). The impedance of a CPE, Z_{CPE} , and the capacitive impedance, Z_C , are defined by these equations:

$$Z_C = \frac{1}{i\omega C} \quad Z_{CPE} = \frac{1}{i\omega Q^n}$$

where ω is the angular frequency (s^{-1}), $i = (-1)$. Q^n is the CPE capacitance (F) where n has a value of 1.0 if the CPE is purely capacitive. n is used as a fitting parameter in this study and has a value of $1.0 < n < 1.2$.

The *VBR* produces a distinctive impedance response consisting of a semicircular Nyquist plot (Z_{im} versus Z_{re} as a function of frequency) (Figure 4a–c). This response resembles the Randles equivalent circuit that is commonly seen for electrochemical biosensors operating in the presence of an added redox species, such as $Fe(CN)_6^{3-/4-}$.^{15,16} The semicircular Nyquist plot for electrochemical biosensors derives from electron transfer to and from the redox species present in the solution. When a redox species is not added, no semicircle is observed. The *VBR* produces a semicircular Nyquist plot *without added redox species*. Instead, the *VBR* channel presents a parallel resistance – dominated by electron conduction through the polymer composite *VBR* – and capacitance – produced by the non-Faradaic charging and discharging of the electrical double layer at the surface of the *VBR*. The semicircular Nyquist plots aids in the precision with which R_{VBR} can be measured – just as it does in electrochemical biosensors that use the diameter of this semicircle – the so-called charge transfer resistance – to transduce target binding.^{17,18,19}

VBR biosensors are able to distinguish between changes in the electrical resistance of the test solution, caused by variations in the salt concentration for example, and the concentration of target molecules present in this solution. Information on the electrical conductivity of the solution is contained in R_{soln} whereas the concentration of target protein is encoded by R_{VBR} . Virtually no cross-talk occurs between these two circuit elements. For example, Nyquist plots (Z_{im} versus Z_{re} as a function of frequency) for a *VBR* in three concentrations of PBS buffer (1x PBS, 2.5x PBS and 5x PBS) show the same $R_{VBR} = R_{VBR,HSA} - R_{VBR,buffer}$ signal for 75 nM HSA (Figure 4e) independent of the salt concentration ($[NaCl]$) over the range of 134 to 670 mM. Notably, R_{soln} decreases dramatically with increasing salt concentration (Figure 4d).

The complementary experiment is to vary [HSA] in a 1x PBS buffer solution (Figure 4f). Here, Nyquist plots are shown for five buffer solutions containing [HSA] = 0 nM, 70 nM, 220 nM, 370 nM, and 750 nM. In this case, a quasi-linear increase in R_{VBR} with [HSA] is measured (Figure 4h), and R_{soln} remains constant (Figure 4g). This property of *VBRs* – the ability to parse changes in impedance due to the solution resistance and target binding – provides an enormous advantage in terms of the application of this biosensor technology to body fluids where salt concentrations are unknown and uncontrolled.

VBR performance was evaluated for the detection of HSA using 20 *VBRs* in order to assess sensor-to-sensor reproducibility and coefficient-of-variance (CoV) to determine their practicality for single use biosensors. Two methods for analyzing *VBR* impedance data are also assessed here. The first method was previously used for non-faradaic impedance biosensors where the signal-to-noise guided the selection of a single frequency at which either Z_{im} or Z_{re} was calculated by, for example, $Z_{re,HSA} - Z_{re}^{0}$.²⁰ Using this approach, the sensing signal at 5 Hz was selected. The second method exploits a range of impedance data across 40–50 discrete frequencies and employs a fit to the equations of Table 1 to determine R_{VBR} . Method 1 will afford more rapid analysis because impedance data at a

single frequency is required. Method 2 requires longer analysis times; however, the approach has the potential to provide for higher precision and reduced noise for an assay, but can this advantage be demonstrated? To answer this question, the two methods were compared for three independent *VBR* biosensors ($N = 3$) at each HSA concentration from 7.5 nM to 750 nM to evaluate sensor-to-sensor reproducibility. In addition, two sensors ($N=2$) were tested at 900 nM [HSA].

The performance of Methods 1 and 2 are summarized in the plots of Figure 5a and b, respectively. The main conclusion is that there is little difference in the performance of these two methods in terms of sensitivity, precision, and noise. Both $Z_{re, 5Hz}$ (Method 1) and R_{VBR} (Method 2) track increases in the HSA concentration from 7.5 nM to 900 nM HSA, saturating at close to 900 nM. These two calibration plots are both fitted with the Hill equation, which is frequently used to model biosensor response:²¹

$$\Delta Z_{re} = \Delta Z_{re, lim} + \frac{\Delta Z_{re,0} - \Delta Z_{re, lim}}{1 + \left(\frac{C_{HSA}}{K_D}\right)^h}$$

The best fit to the Hill equation for the Z_{re} calibration plot results in $Z_{re, lim} = 250 \pm 40 \Omega$, $Z_{re,0} = 16 \pm 5 \Omega$, $K_D = 480 \pm 120$ nM, $h = 1.6 \pm 0.3$, and $R^2 = 0.97$. Fit to the Hill equation for the $R_{channel}$ calibration plot results in $R_{VBR, lim} = 250 \pm 30 \Omega$, $R^0_{VBR} = 20 \pm 5 \Omega$, $K_D = 410 \pm 60$ nM, $h = 1.9 \pm 0.3$, and $R^2 = 0.98$. These data provide no justification for the use of multiple analysis frequencies (Method 2) as compared with a single, S/N-selected, analysis frequency (Method 1). Apparent K_D values are identical within experimental error. Values of h , which indexes the degree of cooperativity in target binding to virus particles, are also identical and equal to 1.6, which indicates significant cooperativity for phage binding to HSA in this system.

The origin of the *VBR* impedance signal is of interest, and remains the subject of investigation. Either of two signal transduction mechanisms could reasonably account for our observations: First, the PEDOT-PSS can function as a p-type organic semiconductor field effect transistor (FET).^{22,23} In this case, an increase in R_{VBR} with [HSA] is accounted for by the binding of a positively charged target molecule to the *VBR*, leading to depletion of majority carriers and an increase in impedance. But HSA has an isoelectric point, $pI = 5.3$,²⁴ and our PBS buffer has $pH = 8.0$., so the HSA in these experiments is expected to have an overall negative charge, not a positive charge, at this pH . The binding of HSA to the PEDOT *VBR* should therefore cause the accumulation of majority carriers, reducing its electrical impedance, which is contrary to our experimental observations. As demonstrated in Figure 4e, the signal amplitude observed for HSA is unaffected by increases in the salt concentration of the test solution from 1x PBS to 5x PBS. This observation suggests that an electric field effect is not involved in the signal transduction process, since the Debye length in these buffer solutions is both very small (2–8 Å) and variable.

A second, previously observed mechanism involves the disruption of long range ordering in the PEDOT-PSS polymer chains. For example, bulky intercalators such as tosylate anions

can cause an increase in electrical resistance,²⁵ or “secondary dopants” – or by “secondary dopants” – including diethylene glycol,¹⁷ olyethylene glycol,¹⁶ and dimethyl sulfoxide¹⁶ – that lubricate the motion of polymer chains thereby promoting a higher degree of long range ordering and a lower electrical resistance. HSA is readily classified as falling into the first category of bulky, structure disrupter. This description qualitatively explains the increases in resistance seen for *VBR*s upon exposure to HSA reported here. Furthermore, this model is consistent with the observed impedance signal for HSA measured at *VBR*s remaining unrelated to the salt concentration of the test solution. More work needs to be done with other analytes and solutions to cement our understanding of the *VBR* signal transduction mechanism.

In addition to sensitivity and reproducibility, selectivity and speed are the two other attributes important for biosensors. The selectivity of *VBR* biosensors was examined with two control conditions: 1) a *VBR* virus-PEDOT film containing HSA-binding virus measured for binding to 750 nM BSA protein, which is closely matched to HSA in terms of both size (both 66.5 kDa) and amino acid sequence (76% homologous)²⁶, and, 2) a *VBR* virus-PEDOT film containing the negative control STOP4 virus, which has no displayed peptide ligands, in the presence of 750 nM HSA protein. The sensing signal is described as

$R_{VBR} = R_{VBR,HSA} - R_{VBR,PBS}$, determined by fitting the impedance data with the equivalent circuit of Table 1. Both control *VBR* biosensors show less than $\sim 1 \Omega$ in of change (in either R_{VBR} or Z_{re}) in comparison to $\sim 200 \Omega$ resistance increase for HSA-virus-PEDOT films against 750 nM HSA. The impedance response for *VBR*s gives excellent binding signal specific to HSA at 200x over background (Figure 6a). Real-time *VBR* measurements (Figure 6b) allow the response time of these devices to be directly measured. We observe a rapid (3 – 30s) step-wise increase in Z_{re} followed by near instantaneous settling of Z_{re} at the concentration-appropriate value (Figure 6b). This constitutes a near ideal response function for a biosensor and demonstrates the potential utility of *VBR*s for point-of-care applications.

The *VBR* simplifies the problem of electrically communicating with virus particles, and importantly, extracting valuable information in this process. Communication takes the form of an increase in the electrical impedance of the virus-PEDOT *VBR* in the presence of a target protein disease marker, relative to the impedance measured in a pure buffer solution. This impedance increase of up to 200 Ω signals the degree to which virus-displayed peptides have recognized and bound a particular target protein, leading to precise and highly reproducible measurement of the concentration of this target molecule. The *VBR* is able to by-pass a ubiquitous noise source in electrical or electrochemical biosensing: the variable electrical impedance of the solution itself.

Supplementary Material

Refer to Web version on PubMed Central for supplementary material.

Acknowledgments

R.M.P. and A.F.O acknowledge support through the NSF Graduate Research Fellowships Program (GRFP) (Award DGE-1321846). In addition, the authors acknowledge support from the National Cancer Institute of the NIH

(1R33CA206955-01), PhageTech Inc (PHAGE-203015), and the Chao Family Comprehensive Cancer Center, UC Irvine. FE-SEM and TEM data were acquired using the instrumentation of the LEXI (lexi.eng.uci.edu/) and IMRI (ps.uci.edu/imri/) facilities at UCI. In addition, the assistance of Dr. Mark Richardson with EDOT purification is gratefully acknowledged.

References Cited

1. Simon DT, Gabrielsson EO, Tybrandt K, Berggren M. *Chem Rev.* 2016; 116:13009–13041. [PubMed: 27367172]
2. Lanzani G. *Nat Mat.* 2014; 13:775–776.
3. Liao C, Zhang M, Yao MY, Hua T, Li L, Yan F. *Adv Mat.* 2015; 27:7493–7527.
4. Cohen-Karni T, Quan Q, Li Q, Fang Y, Lieber CM. *Nano Lett.* 2010; 10:1098–1102. [PubMed: 20136098]
5. Tzahi, Cohen-Karni T., Casanova, D., Cahoon, JF., Qing, Q., Bell, DC., Lieber, CM. *Nano Lett.* 2012; 12:2639–2644. [PubMed: 22468846]
6. Pankratova G, Hasan K, Leech D, Hederstedt L, Gorton L. *Electrochem Commun.* 2017; 75:56–59.
7. Yuan Y, Shin H, Kang C, Kim S. *Bioelectrochem.* 2016; 108:8–12.
8. Kaneko M, Ishikawa M, Hashimoto K, Nakanishi S. *Bioelectrochem.* 2017; 114:8–12.
9. Donovan KC, Arter JA, Weiss GA, Penner RM. *Langmuir.* 2012; 28:12581–12587. [PubMed: 22856875]
10. Arter JA, Diaz JE, Donovan KC, Penner RM, Weiss GA. *Anal Chem.* 2012; 84:2776–2783. [PubMed: 22339784]
11. Donovan KC, Arter JA, Pilolli R, Cioffi N, Weiss GA, Penner RM. *Anal Chem.* 2011; 83:2420–2424. [PubMed: 21388148]
12. Xue W, Jiang X, Harima Y. *Synth Met.* 2010; 160:803–807.
13. Harris PD, Arnold WM, Andrews MK, Partridge AC. *Sens Actuat B-Chem.* 1997; 42:177–184.
14. Bruschi P, Cacialli F, Nannini A, Neri B. *J Appl Phys.* 1994; 76:3640–3644.
15. Yu L, Zhang Y, Hu C, Wu H, Yang Y, Huang C, Jia N. *Food Chem.* 2015; 176:22–26. [PubMed: 25624202]
16. Eissa S, Siaj M, Zourob M. *Biosens Bioelectron.* 2015; 69:148–154.
17. Zhang J, Wu DZ, Cai SX, Chen M, Xia YK, Wu F, Chen JH. *Biosens Bioelectron.* 2016; 75:452–457. [PubMed: 26363493]
18. Li N, Brahmendra A, Veloso AJ, Prashar A, Cheng XR, Hung VWS, Guyard C, Terebiznik M, Kerman K. *Anal Chem.* 2012; 84(8):3485–3488. [PubMed: 22424137]
19. Gao Z, Deng H, Shen W, Ren Y. *Anal Chem.* 2013; 85(3):1624–1630. [PubMed: 23323518]
20. Ogata AF, Edgar JM, Majumdar S, Briggs JS, Patterson SV, Tan MX, Kudlacek ST, Schneider CA, Weiss GA, Penner RM. *Anal Chem.* 2017; 89:1373–1381. [PubMed: 27989106]
21. Xiao Y, Jiang W, Zhang F. *ACS Synth Biol.* 2017; 6(10):1807–1815. [PubMed: 28683543]
22. Gao Z, Deng H, Shen W, Ren Y. *Anal Chem.* 2013; 85(3):1624–1630. [PubMed: 23323518]
23. Chu CH, Sarangadharan I, Regmi A, Chen YW, Hsu CP, Chang WH, Lee GY, Chyi JI, Chen CC, Shiesh SC, Bin Lee G, Wang YL. *Sci Rep.* 2017; 7(1)
24. Dockal M, Carter DC, Ru F. *October.* 1999; 274(41):29303–29310.
25. Meier AR, Bahureksa WA, Heien ML. *J Phys Chem C.* 2016; 120:21114–21122.
26. Majorek KA, Porebski PJ, Dayal A, Zimmerman MD, Jablonska K, Stewart AJ, Chruszcz M, Minor W. *Mol Immunol.* 2012; 52:174–182. [PubMed: 22677715]

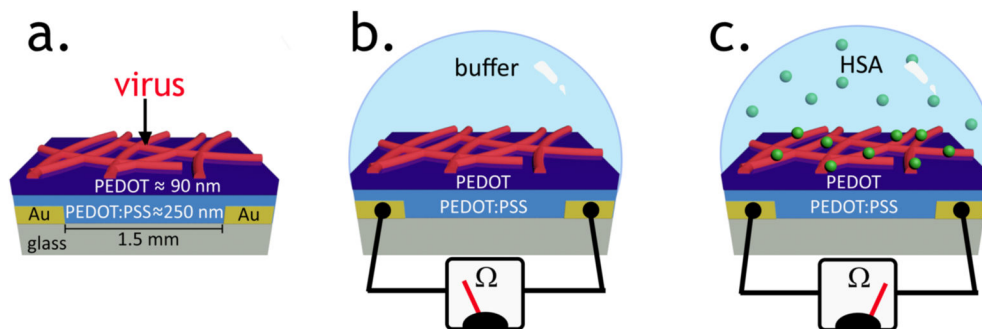


Figure 1.

The *Virus BioResistor* (*VBR*). a) Schematic diagram of a *VBR* showing critical components and dimensions. b) A buffered salt solution alters the solution resistance, R_{soln} , but not the resistance of the *VBR* channel, R_{VBR} . c) In the presence of a target protein (HSA in this case), R_{VBR} is increased, enabling determination of its concentration.

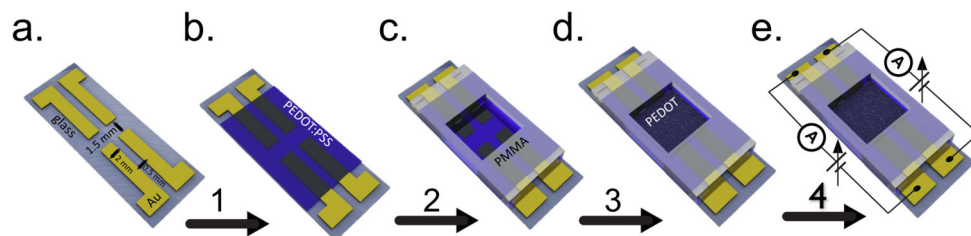


Figure 2.

VBR biosensor fabrication. a) Two pairs of gold-electrodes from which two *VBR*s are prepared. The gold electrodes have width of 2 mm and their separation of 1.5 mm defines the channel length of these devices. The two pairs of gold electrodes are separated by 0.5 mm. b) A layer of PEDOT:PSS is spin-coated onto the gold-electrode device and baked for 1 h at 90 °C. c) A 2 mm × 2 mm PMMA cell is attached defining the area of the bioaffinity layer. d) A virus-PEDOT top layer is electropolymerized on top of the PEDOT:PSS bottom layer by using $\approx 100 \mu\text{L}$ of plating solution and applying two oxidizing voltammetric scans. e) The virus-PEDOT plating solution is removed, and the cell is rinsed. Electrodes are used to enable impedance measurements at each of the two *VBR* sensors. One background impedance measurement is acquired in buffer, and a second in a solution containing added HSA. The calculated R_{VBR} is used to determine the HSA concentration in this sample with reference to a calibration curve.

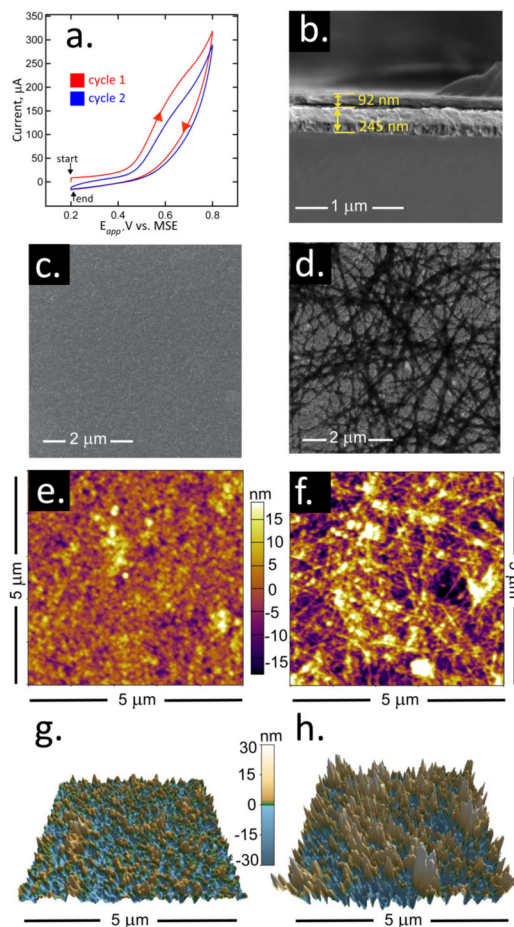


Figure 3. Electrodeposition and SEM/AFM characterization of virus-PEDOT bioaffinity layers. (a) Electrodeposition of a virus-PEDOT film on a PEDOT-PSS film using cyclic voltammetry (50 mV/s). The virus-PEDOT top layer is prepared by two cycles from an aqueous virus-EDOT solution containing 2.5 mM EDOT, 12.5 mM LiClO₄, and 8 nM HSA phage. (b) cross sectional scanning electron microscopy (SEM) image of a PEDOT-PSS/virus-PEDOT film. The PEDOT-PSS bottom layer and virus-PEDOT top layer can be distinguished. (c) Plan view SEM image of a PEDOT only film (no virus) prepared by two consecutive cycles of deposition in aqueous EDOT solution containing 2.5 mM EDOT, 12.5 mM LiClO₄. (d) Plan view SEM image of a virus-PEDOT film prepared as described in (a). (e,f,g,h) Atomic force microscopy (AFM) images of PEDOT films (e,g) and virus-PEDOT films (f,h). The same AFM image data are represented in two ways: (e,f) shows height versus position data while (g,h) show a three-dimensional rendering of these the same data shown in (e,f). The rms roughness for PEDOT and virus-PEDOT films are ≈ 5 nm and ≈ 10 nm, respectively.

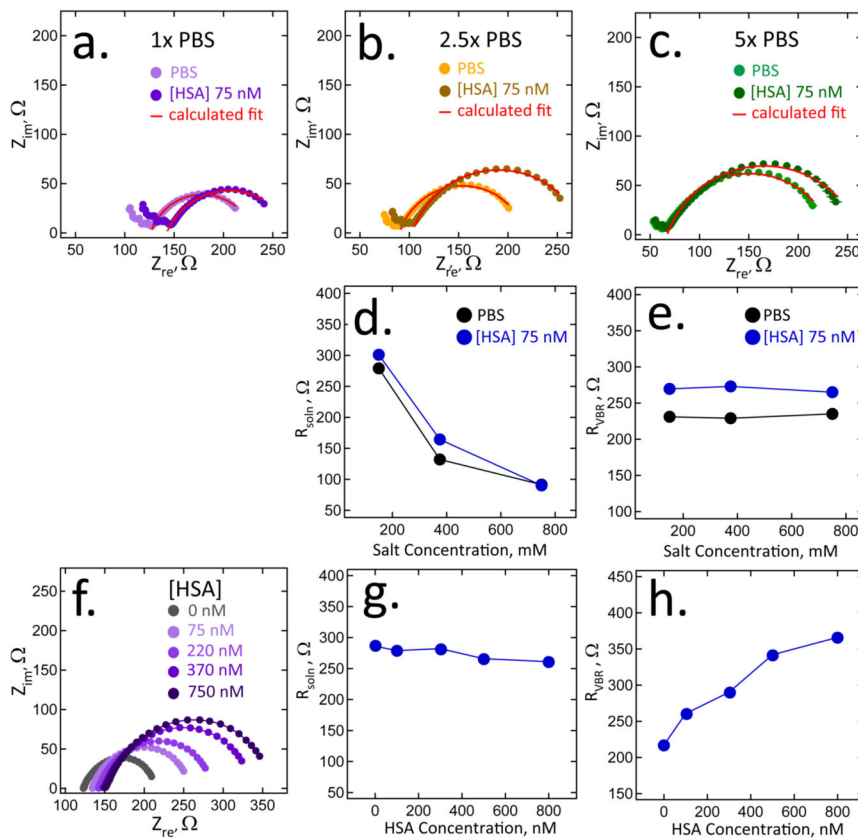


Figure 4. Orthogonal measurement of R_{soln} and R_{VBR} using a VBR biosensor. Nyquist plots summarizing the impedance response of VBR s from 1 Hz to 10 kHz with equivalent circuit fits (red traces). (a,b,c) VBR s in solutions of run buffer of: a). 1x PBS (purple), b). 2.5x PBS (yellow), c). 5x PBS (green), before and after exposure to 75 nM HSA in the same buffer. (d,e). Plots of R_{soln} and R_{VBR} as a function of buffer concentration extracted from the data of a,b, and c. Shown are the values of these two circuit elements in pure buffer, and in buffer with added 75 nM HSA, as indicated. (f,g,h) Experiment in which the HSA concentration is increased from 0 nM (1x PBS) to 750 nM (in 1x PBS) showing the invariance of R_{soln} and the linear increase in R_{VBR} .

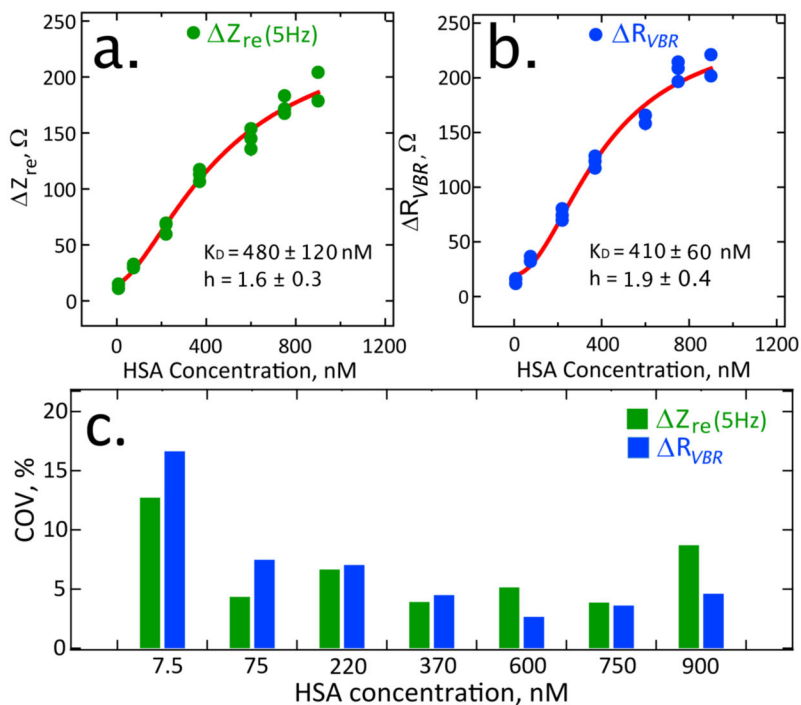


Figure 5. Calibration plots for 20 VBRs exposed to HSA concentrations 7.5 nM – 900 nM generated by two methods (5a) sensing signal Z_{re} , measured at 5 Hz, versus concentration (5b) sensing signal defined as R_{VBR} , versus concentration. At each of seven concentration points, three data point for three different VBR sensors are plotted here with error bars defined as the standard deviation, $\pm 1\sigma$. The exception is the 900 nM concentration point where just two sensors were used, and two data points are shown. It should be noted that these three data points are not all seen at all concentrations, since some are superimposed on others. Impedance data for HSA exposed to virus-PEDOT films containing HSA phage is fitted to the hill equation (red line). c) compares the CoV% for the signals from two methods obtained by the variation in signal generated by three devices exposed to concentrations [HSA] = 7.5 nM – 900 nM.

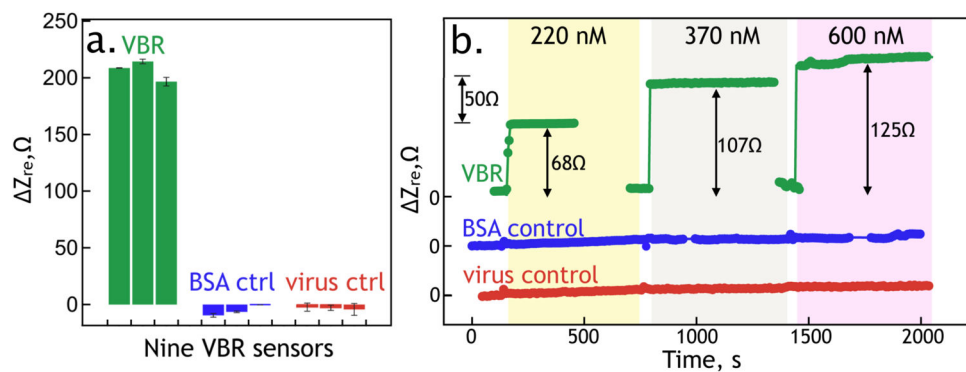
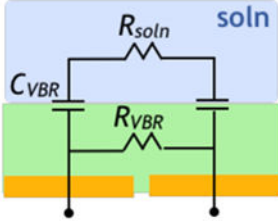
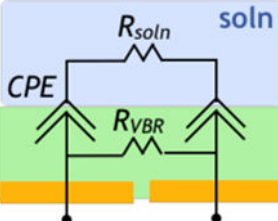


Figure 6.

VBR specificity and speed. a). A specificity assay. Blue bars represent three *VBR*s with PEDOT films containing HSA binding phage exposed to 750 nM HSA; Red bars show the response to a 750 nM BSA solution of three *VBR*s containing HSA binding phage; Green bars show the response to a 750 nM HSA solution for three *VBR*s containing STOP4 phage that have no affinity for HSA. b). Real time *VBR* sensing data. Responses for three *VBR* sensors are shown for [HSA] exposures of 220, 370, and 600 nM that show response times of 30 s, 3 s, and 3 s, respectively. The specificity assay summarized in (a) are also repeated here, in real-time sensing format, again showing no measurable responses.

Table 1

Equivalent circuits and equations representing the electrical response of a *VBR* biosensor.

Eq. Circuit ^a	
$Z_{re} =$	$\frac{R_{VBR}R_{soln}(R_{VBR} + R_{soln}) + \frac{R_{VBR}}{\omega^2 C_{VBR}}}{(R_{VBR} + R_{soln})^2 + \frac{1}{\omega^2 C_{VBR}}}$
$Z_{im} =$	$\frac{\frac{R_{VBR}^2}{\omega C_{VBR}}}{(R_{VBR} + R_{soln})^2 + \frac{1}{\omega^2 C_{VBR}}}$
Eq. Circuit ^b	
$Z_{re} =$	$\frac{R_{VBR}[1 + Q_{VBR}\omega^n(2R_{VBR} + R_{soln})\cos\frac{\pi n}{2} + R_{soln}Q_{VBR}^2\omega^{2n}(R_{soln} + R_{VBR})]}{Q_{VBR}\omega^n(R_{soln} + R_{VBR})[(R_{soln} + R_{VBR})Q_{VBR}\omega^n + 2\cos\frac{\pi n}{2}] + 1}$
$Z_{im} =$	$\frac{-R_{VBR}^2\omega^2 Q_{VBR}\sin\frac{\pi n}{2}}{Q_{VBR}\omega^n(R_{soln} + R_{VBR})[(R_{soln} + R_{VBR})Q_{VBR}\omega^n + 2\cos\frac{\pi n}{2}] + 1}$

^aCapacitive equivalent circuit,

^bEquivalent circuit with constant phase elements (CPEs).